ELSEVIER

Natural convection to air from an array of vertical parallel plates with discrete and protruding heat sources

M. Fujii
Institute of Advanced Material Study, Kyushu University, Kasuga, Fukuoka, Japan

S. Gima
Department of Mechanical Systems Engineering, University of the Ryukyus, Okinawa, Japan

T. Tomimura and X. Zhang
Institute of Advanced Material Study, Kyushu University, Kasuga, Fukuoka, Japan

Numerical and experimental studies are carried out on natural convection heat transfer to air from an array of vertical parallel plates with protruding and discrete heat sources, such as IC packages. Two-dimensional (2-D) Navier–Stokes and energy equations including heat conduction through the plates and heat sources are numerically solved under the conditions of modified Grashof number $Gr^* = 2.3 \times 10^3 \sim 8.8 \times 10^5$ and plate height to spacing ratio $L = l/h = 8 \sim 30$. The numerical solutions agree well with the experimental values except for the large aspect ratio $L = 30$, where the three-dimensional (3-D) effects become significant. A correlation expression for the local Nusselt number is proposed; it can predict the protrusion surface temperature within $\pm 20\%$ error. A method for estimating the maximum inner temperature of the heat source is proposed, and the thermally optimum spacing of the parallel plates is discussed.

Keywords: heat transfer; natural convection; heat conduction; numerical analysis; parallel plates; electronic equipment; IC package

Introduction

Among various modes of the cooling technologies for electronic equipment, natural convective air cooling has been given much more attention because of its inherent high reliability. Many studies have been carried out on natural convection heat transfer from vertical parallel plates in relevance to the optimum thermal design of such a cooling system. Bodoia and Osterle (1962), Aung et al. (1972), Aihara (1973), Miyatake and Fujii (1974), Bar-Cohen and Rohsenow (1984), Webb and Hill (1989) and Kim et al. (1991) have reported experimental and/or numerical results with respect to such a problem. Nakayama and Hirooka (1986), Fujii and Tomimura (1988) and Beckermann et al. (1994) have investigated the heat transfer characteristics of IC boards in more detail by taking into account the effects of both discreteness and protrusions of these heat sources. Related studies are reviewed by Incropera (1988).

The authors continued a series of studies on natural convection heat transfer to air from an array of vertical parallel plates. The heat transfer and flow characteristics for plane plates were clarified theoretically and experimentally (Fujii et al. 1994a, 1994b), and for the plates with many protruding heat sources, the effects of the protrusions on induced flow rates and heat transfer were clarified experimentally (Fujii et al. 1992).

The present paper describes the numerical and experimental results of natural convection to air from an array of vertical parallel plates with discrete and protruding heat sources. The effects of these geometrical and thermal conditions on heat transfer characteristics are clarified, and further are discussed as the method for estimating the chip temperatures of the practical IC packages and the thermally optimum spacing of such parallel plates as IC boards.

Numerical analysis

Figure 1 shows the physical model and coordinate system. An infinite number of plates are placed in a vertical parallel arrangement with an equal spacing h. Each plate has the same height l and thickness b. On one surface of the plate are mounted eighteen protruding heat sources with separation s_p, and each heat source has the same length l_p, height h_p and generates heat Q_c $(= Q/18)$, where Q is the total heat generation rate per plate. Two kinds of heating conditions are consid-

Address reprint requests to Prof. M. Fujii, Institute of Advanced Material Study, Kyushu University, Kasuga, Fukuoka 816, Japan.

Received 7 August 1995; accepted 18 March 1996.

Int. J. Heat and Fluid Flow 17: 483–490, 1996

655 Avenue of the Americas, New York, NY 10010

0142-727X/96/$15.00
PII S0142-727X(96)00051-1

ered. The first is uniform heat generation in each source. In the second, to simulate the practical IC packages, the heat generation Q_c is concentrated within a very small volume [($l_p/5$ long) $\times$ ($h_p/28$ thick)] in each source, where the volume size is chosen by referring to the DIP-type model packages.

In the present numerical analysis,

(1) The heat conduction in the base plate as well as in the heat sources is taken into account with an assumption of a same thermal conductivity λ_s.
(2) The air of Pr = 0.7 and an inlet temperature T_i is assumed to flow into the array with a uniform velocity u_m.
(3) The radiative heat transfer among the plates and the ambient is not accounted for.
(4) The solution domain is chosen to be the region bounded by the broken line in Figure 1; whereas, a periodic boundary condition is imposed with respect to the temperature and heat flux at the plate surface.

Note that the measured longitudinal (x-directional) temperature distributions in the inner three (#2, 3, and 4) of the five rows of the plates are almost the same, and the maximum difference is 7%, even for $L = 30$. The application of the periodic boundary condition to the present analysis, therefore, is considered to be valid as a first approximation. In the following, the surface on which the heat sources are mounted is named as the front surface ($y = 0$), and the other the back ($y = -b, h$).

Two-dimensional (2-D) Navier–Stokes and energy equations can be applied to the above model. Introducing stream function ψ and vorticity ω and using the Boussinesq approximation, the governing equations are expressed in dimensionless forms as follows:

$$-\Omega = \frac{\partial}{\partial X}\left(\frac{\partial \Psi}{\partial X}\right) + \frac{\partial}{\partial Y}\left(\frac{\partial \Psi}{\partial Y}\right) \tag{1}$$

$$\frac{\partial}{\partial X}\left(\Omega\frac{\partial \Psi}{\partial Y}\right) - \frac{\partial}{\partial Y}\left(\Omega\frac{\partial \Psi}{\partial X}\right) = -4\frac{\mathrm{Gr}^*}{\mathrm{Re}^2}\frac{\partial \theta_f}{\partial Y} + \frac{2}{\mathrm{Re}}\left[\frac{\partial}{\partial X}\left(\frac{\partial \Omega}{\partial X}\right) + \frac{\partial}{\partial Y}\left(\frac{\partial \Omega}{\partial Y}\right)\right] \tag{2}$$

$$\frac{\partial}{\partial X}\left(\theta_f\frac{\partial \Psi}{\partial Y}\right) - \frac{\partial}{\partial Y}\left(\theta_f\frac{\partial \Psi}{\partial X}\right) = \frac{2}{\mathrm{Re\,Pr}}\left[\frac{\partial}{\partial X}\left(\frac{\partial \theta_f}{\partial X}\right) + \frac{\partial}{\partial Y}\left(\frac{\partial \theta_f}{\partial Y}\right)\right] \tag{3}$$

The dimensionless heat conduction equation in the base plate and the heat source is given as:

$$\frac{\partial^2 \theta_{s,p}}{\partial X^2} + \frac{\partial^2 \theta_{s,p}}{\partial Y^2} + f\frac{2L}{18RH_pL_p} = 0 \tag{4}$$

where $f = 1$ for the heating region and $f = 0$ for the rest. When the source is locally heated, H_pL_p in Equation 4 is replaced by $(H_p/28) \times (L_p/5)$.

Notation

A one side surface area of plate, m^2
A_p appropriate heat transfer area, Equation 13, m^2
B dimensionless plate thickness, b/h
b plate thickness, m
F_w dimensionless normal heat flux from heat source surface to air, $-\lambda(\partial T/\partial n)/q_w$
Gr* modified Grashof number, Equation 6
g gravitational acceleration, m/s^2
H_p dimensionless heat source height, Equation 6
h plate spacing, m
h_e effective plate spacing, $h - h_p$, m
h_{opt} thermally optimum spacing, m
h_p heat source height, m
L dimensionless plate height (aspect ratio), Equation 6
L_p dimensionless heat source length, Equation 6
l plate height, m
l_i distance between the plate leading edge and the lowermost heat source, Figure 1, m
l_o distance between the plate trailing edge and the uppermost heat source, Figure 1, m
l_p heat source length, m
N dimensionless normal coordinate, Equation 6
n normal coordinate, m
Nu local Nusselt number, Equation 9
Pr Prandtl number, Equation 6
Q total heat generation rate per plate, W
Q_c heat generation rate of each heat source, W
Q_p heat transferred to the heat source surface, Equation 13, W
q_w mean heat flux, Equation 7, W/m^2
R thermal conductivity ratio of plate to air, Equation 6
R_{cw} equivalent thermal resistance, K/W
Re Reynolds number, Equation 6
s_p heat source pitch, m
T absolute temperature, K
T_c maximum temperature in the heat source, K
T_i inlet temperature, K
U dimensionless velocity component in X-direction, u/u_m
u velocity component in x-direction, m/s
u_m mean velocity in x-direction, m/s
v velocity component in y-direction, m/s
X dimensionless vertical coordinate, Equation 6
x vertical coordinate, m
Y dimensionless horizontal coordinate, Equation 6
y horizontal coordinate, m

Greek

β coefficient of thermal expansion, $1/T_i$, K^{-1}
ΔY dimensionless distance between the protrusion surface and the concentrated heat source, $\Delta y/h$, Figure 8
Δy distance between the protrusion surface and the concentrated heat source, m
θ dimensionless temperature, Equation 6
θ_c dimensionless maximum temperature in the protruding heat source
κ thermal diffusivity, m^2/s
λ thermal conductivity, W/mK
ν kinematic viscosity, m^2/s
ξ parameter, Equation 16, m^{-5}
Φ dimensionless variable, Equation 10
Ψ dimensionless stream function, Equation 6
ψ stream function, m^2/s
Ω dimensionless vorticity, Equation 6
ω vorticity, s^{-1}

Subscripts

f air
$l/2$ midheight
p protruding heat source
s plate
w heat source surface

The boundary conditions for the case of uniform heat generation in each source are given by

$$
\begin{aligned}
&X=0, 0\le Y\le 1 : \Psi=Y,\quad \Omega=0,\quad \theta_f=0\\
&\quad -B\le Y\le 0 : \theta_s=0\\
&X=L, 0\le Y\le 1 : \Psi=\Psi_{ex},\quad \Omega=\Omega_{ex},\quad \theta_f=\theta_{f,ex}\\
&\quad -B\le Y\le 0 : \theta_s=\theta_{s,ex}\\
&0\le X\le L, Y=0 : \text{for nonheating region}\\
&\qquad \Psi=0,\ \Omega=-\frac{\partial^2\Psi}{\partial Y^2},\quad \theta_f(X,0)=\theta_s(X,0),\quad \frac{\partial\theta_f}{\partial Y}=R\frac{\partial\theta_s}{\partial Y}\\
&\qquad \text{for heating region, } \theta_s(X,0)=\theta_p(X,0),\quad \frac{\partial\theta_s}{\partial Y}=\frac{\partial\theta_p}{\partial Y}\\
&0\le X\le L, Y=1 : \Psi=1,\ \Omega=-\frac{\partial^2\Psi}{\partial Y^2},\\
&\qquad \theta_f(X,1)=\theta_s(X,1)=\theta_s(X,-B),\quad \frac{\partial\theta_f}{\partial Y}=R\frac{\partial\theta_s}{\partial Y}
\end{aligned}
$$

at the heat source surface: $\Psi=0,\quad \Omega=\pm\dfrac{\partial^2\Psi}{\partial N^2},\quad \theta_f(X,Y)=\theta_p(X,Y),\quad \dfrac{\partial\theta_f}{\partial N}=R\dfrac{\partial\theta_p}{\partial N}$ (5)

where the boundary values with subscript ex are obtained by an extrapolation from the corresponding values on the inner two nodes. This method is proved to be effective as an exit flow boundary condition and provide a reasonable result (Tomimura and Fujii 1988). The dimensionless variables in the above equations are defined by

$$
X=\frac{x}{h},\quad Y=\frac{y}{h},\quad N=\frac{n}{h},\quad L=\frac{l}{h},\quad B=\frac{b}{h},\quad H_p=\frac{h_p}{h},
$$

$$
L_p=\frac{l_p}{h},\quad \theta=\frac{T-T_i}{q_w h/\lambda_f},\quad \Psi=\frac{\psi}{u_m h},\quad \Omega=\frac{\omega}{u_m/h},
$$

$$
R=\frac{\lambda_s}{\lambda_f},\quad \mathrm{Pr}=\frac{\nu}{\kappa},\quad \mathrm{Re}=\frac{u_m 2h}{\nu},\quad \mathrm{Gr}^*=\frac{g\beta q_w h^4}{\lambda_f\nu^2} \qquad (6)
$$

In the above, the mean heat flux q_w is defined based on the total surface area of the base plate $2A$ as

$$
q_w=\frac{Q}{2A} \qquad (7)
$$

The equations are solved by an upwind finite difference method using a successive substitution scheme. To obtain the solutions for pure natural convection, iterations are necessary with respect to the induced flow rate; i.e., the Reynolds number Re, so that the pressure difference between the exit and the inlet becomes sufficiently small. As for the values of the vorticities and the temperatures at each corner of the protrusions, the arithmetic averages of the respective values extrapolated from those in the X and Y directions are used. To perform accurate calculations for the velocity and temperature profiles near the inlet section and the plate and protrusion surfaces, a nonuniform grid is used. Depending on the parameters, a grid size study on computational meshes up to $392\sim610$ and $88\sim104$ in the X and Y directions is conducted, and grid independence of the numerical results on these numbers of grids is confirmed.

The parameter ranges in the present calculations are shown in Table 1(a). These parameters correspond to the present experimental conditions, which cover the ranges of practical memory boards. Here, the variable R is the ratio of the thermal conduc-

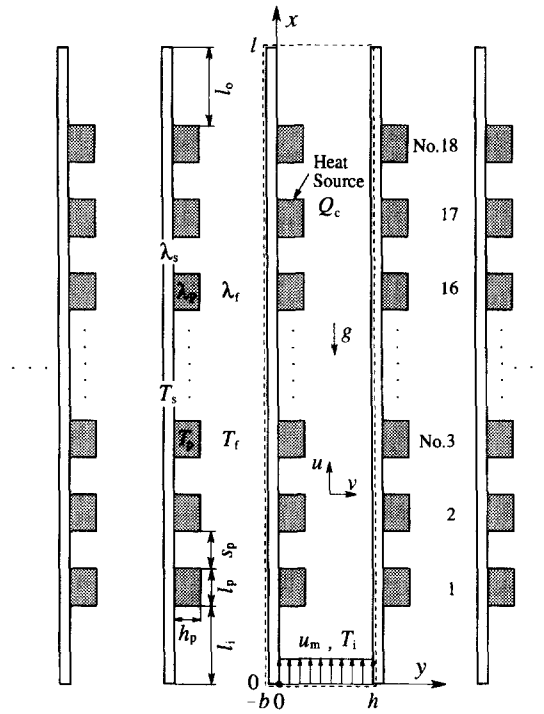

Figure 1 Physical model and coordinate system

Table 1 Parameter ranges

(a) Numerical calculations (Pr=0.71, R=10)				
L [−]	30	20	15	8
B [−]	0.16	0.11	0.08	0.05
H_p [−]	0.5	0.33	0.25	0.14
$L_p=S_p$ [−]	0.75	0.5	0.37	0.2
$L_i=L_o$ [−]	1.875	1.25	1.025	0.5
Gr* [−]	2.3×10^3	2.1×10^4	8.2×10^4	8.8×10^5
($S_p=s_p/h$, $L_i=l_i/h$, $L_o=l_o/h$)				
(b) Experiments (air)				
h mm	9.7	14.7	19.7	34.7
Q, W	5.6	9.6	11.6	13.0
q_w W/m^2	41.5	71.1	85.9	96.2

tivity of the plate and heat source $\lambda_s\ (=\lambda_p)$ to that of air λ_f, and varies from $R = 1 \sim 3$ for usual insulating materials to $R = 11$ for epoxy glass at a room temperature.

In the present numerical calculations, iterations are terminated when the following convergency criterion, $|\Gamma^n_{I,J} - \Gamma^{n-1}_{I,J}|_{max}/|\Gamma^n_{I,J}|_{max} \leq 5 \times 10^{-5}$, is satisfied. Here, Γ represents either Ψ, Ω, or θ, and the subscripts I, J, and max are the node address and the maximum value of Γ, respectively, and the superscript n denotes an iteration step. As a result, the energy balance at the exit is confirmed to have an error within $\pm 2\%$.

Experiments

A schematic of the experimental apparatus is shown in Figure 2. An array of five equally spaced parallel plates is hung vertically in a framework with acrylic side walls. Both sides of the array are closed with acrylic plates to prevent the ambient air from flowing laterally. The plates are numbered from 1 to 5 for convenience.

Figure 3 shows the detail of each plate. The plate is made of glass-epoxy-resin and is 285-mm long, 237-mm wide, and 1.6-mm thick. On one side of each plate, are welded with tin solder the DIP-type (16 pins) ceramic model packages, which are 6.9-mm long, 19.3-mm wide, and 4.8-mm high, in an in-line arrangement of 18 rows and 8 columns. Although there is a 0.9-mm gap between the package bottom surface and the base plate, it is neglected in the numerical analysis. Unlike the practical packages, the chip of the present model package is composed of an electric resistance of about 110 Ω and a diode instead of an integrated circuit.

The package surface temperatures of the central plate at the positions denoted by a circle and the air temperature profiles between the plates at the top exit are measured with 50 μm dia copper-constantan thermocouples. The velocity profiles between the central plates are measured with a backscattering laser-Doppler anemometer (LDA) system at positions A, B, and C. The uncertainties associated with temperature and velocity measurements are ±3 and ±10%, respectively. As the plate, package, and inlet air temperatures are measured within ±0.1°C, and the mean heat flux q_w within ±1%, the error of the present Nu measurement is within ±2%.

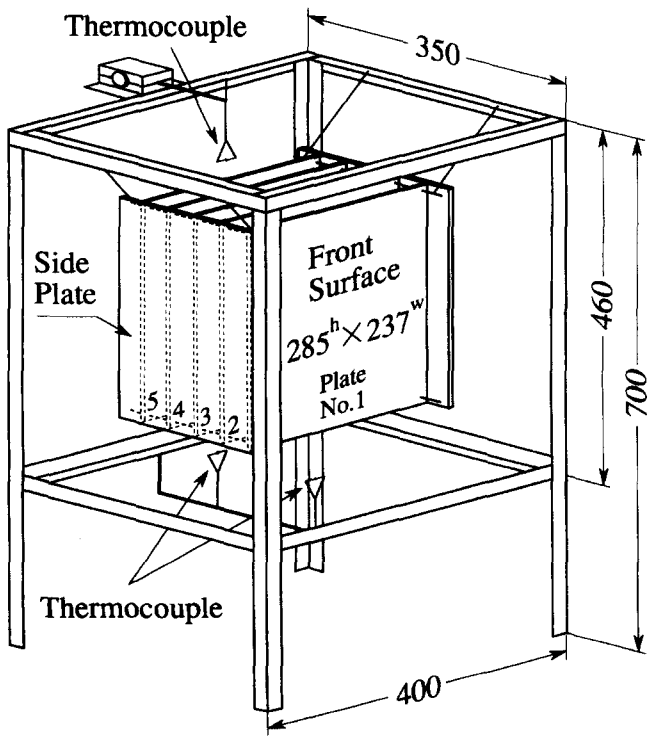

Figure 2 Schematic of the experimental apparatus

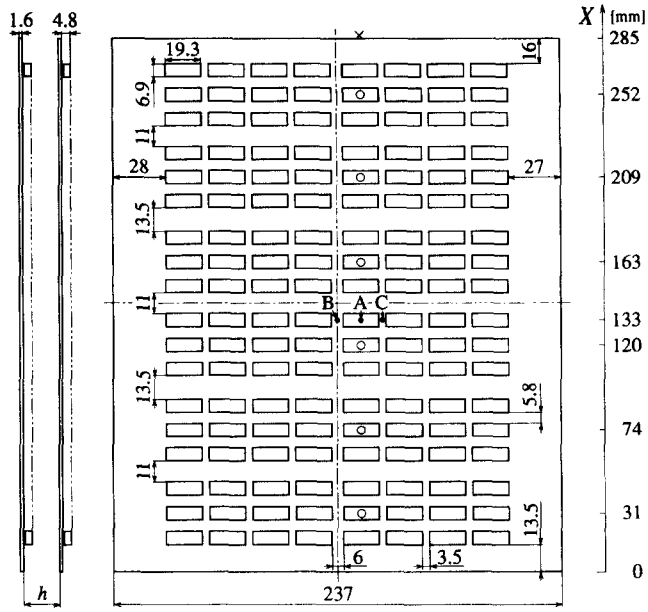

Figure 3 Detail of IC board; the symbols ○ and × represent the measured points of the package surface temperatures and the exit air temperature profile, respectively; A, B, and C stand for the positions of velocity profile measurements with a LDA

The parameter ranges in the experiments are listed in Table 1(b). The plate spacing h is changed stepwise from 9.7 to 34.7 mm. The total heat generation rate Q for each plate is set at the same, and changed from 5.6 to 13.0 W according to the plate spacing to keep the maximum temperature difference between the central plate and the ambient air to be about 25 K. In the following, the numerical results are compared with those measured on the central plate, where the effects of radiative heat transfer among the plates and the ambient can be neglected (Fujii et al. 1992).

Results and discussion

Velocity and temperature profiles between plates

Figures 4(a) and (b) show the effects of the aspect ratio L on the velocity and temperature profiles between the plates. The solid lines in Figure 4(a), which should be compared with the measured profiles at position A, show the calculated results at the same height as the experiments. The numerical solutions agree well with the experimental values, except for the narrowest plate spacing of $L = 30$, where the velocity profiles measured at positions A, B, and C are largely different from each other, and the three-dimensional (3-D) flow becomes significant. Furthermore, because the flow rates between neighboring heat sources are large (especially at the wider space at B), the measured mean velocity u_m is about 35% higher than the numerical one, and, correspondingly, the measured temperature becomes about 38% lower than that. On the contrary, the velocity u_m for the widest plate spacing of $L = 8$ is about 20% lower than the numerical one. These discrepancies are discussed in the next section.

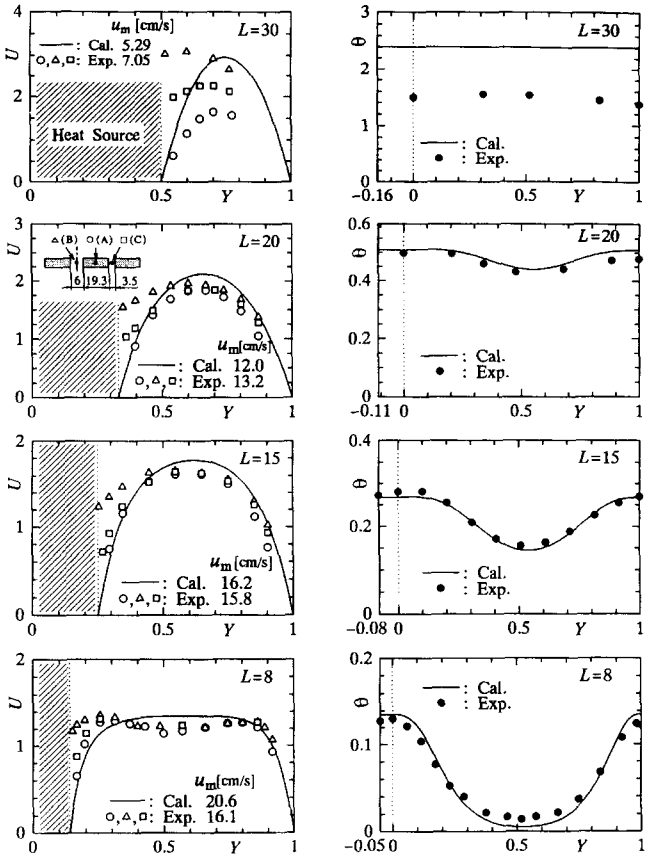

(a) Velocity profiles (b) Temperature profiles

Figure 4 Velocity and temperature profiles between the plates; the symbols ○, △, and □ represent the velocity profiles measured at the central position of the ninth heat source A, at the wider lateral space between neighboring heat sources B, and at the narrower space C, respectively, and the symbol ● represents the temperature profiles measured at the exit (see Figure 3).

Induced flow rates

Figure 5 shows the relation between the dimensionless induced flow rate Re/L and the parameter Gr^*/L. The values calculated and measured are plotted, and the latter is estimated by integrating the velocity profiles. Also included are the results for plane parallel plates (Fujii et al. 1994b). The solid line shows the flow rate corresponding to the fully developed condition (Miyatake and Fujii 1974) given by:

$$\frac{\mathrm{Re}}{L} = 0.690\left(\frac{\mathrm{Gr}^*}{L}\right)^{1/2} \tag{8}$$

Because the flow resistance is increased by the distributed protrusions, the induced flow rates between the plates with the heat sources are lower than those between the plane plates. The flow rates, however, show a tendency to approach the values for the plane plate cases with increasing Gr^*/L, because the effect of protrusions diminishes for a small aspect ratio L. The numerical results agree well with the experimental ones for $L = 15$ and 20. For $L = 8$ ($\mathrm{Gr}^*/L \doteqdot 10^5$), however, the measured value is about 24% lower than the calculated one, and this is also the case for the plane plates. This may be attributed to the reasons that the uniform inlet velocity is assumed in the numerical analysis even

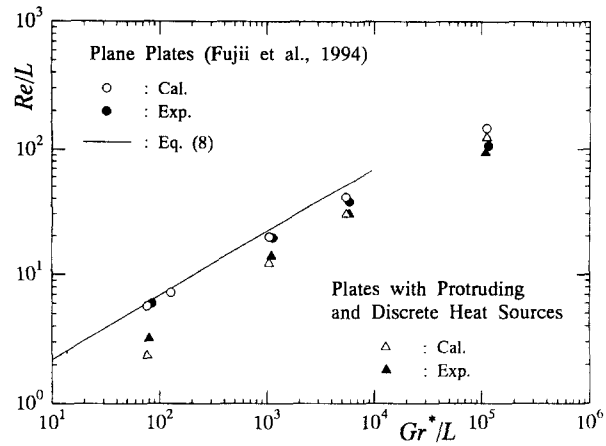

Figure 5 Relation between induced flow rate and Grashof number

for such a small aspect ratio L, and that the zigzag motion of the seeding particles may have reduced the measuring accuracy. Moreover, the velocity is measured at the center channel of the array. Therefore, it is probable that the ambient air could not be supplied smoothly. For the narrowest plate spacing $L = 30$, as mentioned in the induced flow rates section, the velocities between the neighboring heat sources are fairly high as compared with that at the central position of the heat source, so the measured value is about 36% higher than the present result obtained by the 2-D numerical computation.

Streamlines and isotherms

Figures 6(a) and (b) show the calculated results of streamlines and isotherms in the regions $0 \leqq X \leqq 3$ and $12 \leqq X \leqq 15$ for $L = 15$, respectively. From Figure 6(a), it is observed that the recirculating flows are formed between the protrusions, and the flow pattern around each protrusion is almost the same in the region $1 < X < 14$. Corresponding to these flow patterns, the isothermal lines are densely distributed near the protrusion surfaces ($Y = 0.25$) and the plate back surface ($Y = 1$), as shown in Figure 6(b). This means that the heat transfer rates are higher in those regions. As for each protrusion, the local heat transfer rate is higher near the leading edge as compared with that at the trailing edge, and those on horizontal surfaces become low because of the slow recirculating flow between the protrusions. From the present numerical calculations, the quantity of heat transferred from the front surface of the plate and the protrusion surfaces to air is found to be about 51% of the total heat rate Q; that is, the heat Q is almost evenly released from the front and back surfaces of the plate. Although not shown here, the similar tendency with respect to stream and isothermal lines is also obtained for other aspect ratios of L.

Local Nusselt numbers

According to Miyatake and Fujii (1974), the local Nusselt number Nu and the dimensionless variable Φ are defined as

$$\mathrm{Nu} = \frac{q_w}{T_w - T_i}\frac{h_e}{\lambda_f} \tag{9}$$

$$\Phi = \frac{\mathrm{Gr}^*\,\mathrm{Pr}/X}{(\mathrm{Gr}^*\,\mathrm{Pr}/L)^{1/2}} \tag{10}$$

where the effective spacing $h_e = h - h_p$ is used as the characteristics length in Nu, Gr^*, L, and X instead of the plate spacing h.

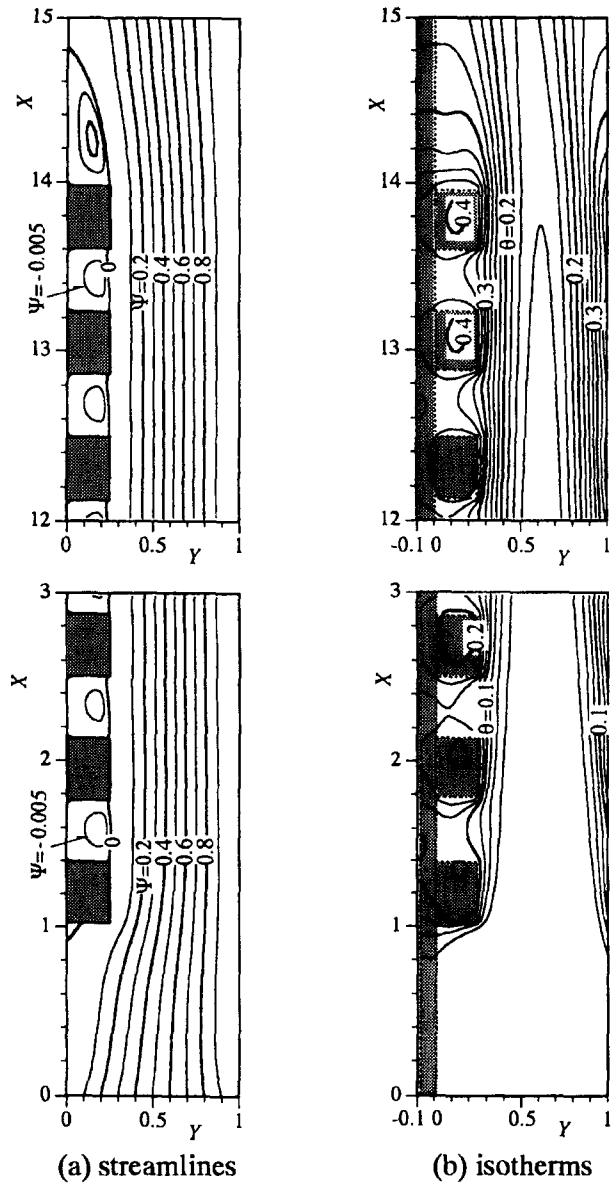

Figure 6 Computed streamlines and isotherms for $L=15$, $Gr^*=8.2\times10^4$, and $Re=444$

Figure 7 shows the relation between Nu and Φ. The experimental results obtained by Nakayama and Hirooka (1986) are also shown. The solid and dotted lines represent the Equations 11 and 12, respectively, which are obtained by modifying the correlation proposed by Miyatake and Fujii (1974) so as to fit the present numerical results:

$$Nu = \frac{\Phi}{6.93}[1-\exp(-4.88\Phi^{-0.66})]$$

for plates with protruding heat sources (11)

$$Nu = \frac{\Phi}{6.93}[1-\exp(-5.72\Phi^{-0.66})]$$

for plane plates (Fujii et al. 1994b) (12)

As seen in Figure 7, for smaller values of Φ, Equation 12 agrees with the asymptotic solution given by Aung (1972) for

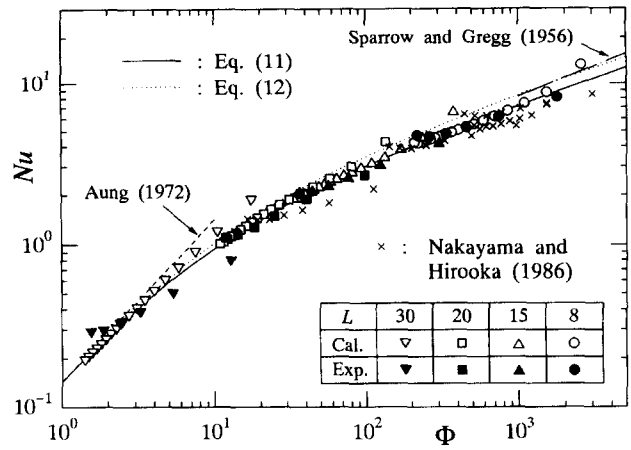

Figure 7 Relation between local Nusselt number and dimensionless variable Φ

fully developed laminar flow between vertical plates. On the other hand, for larger Φ, the equation agrees with the result obtained by Sparrow and Gregg (1956) for laminar flow from a single vertical plate.

Because of reduction of induced flow rate, Equation 11 is about 14% lower than Equation 12 for the range around $\Phi = 10^3$, and the equation agrees with the present experimental values within ±10% except for $L = 30$. The data obtained by Nakayama and Hirooka (1986) show a little lower values than the present. All of the present data for $L = 20, 15, 8$ and those by Nakayama and Hirooka, however, lie within about ±20% around Equation 11, so the equation can be used as a correlation expression for predicting the surface temperature of the protruding heat source.

A series of numerical calculations for $L = 15$, $Gr^* = 8.2\times10^4$, and $R = 1$, 5, and 100 is also conducted. From the results, it is clarified that, compared with Equation 11, the local Nusselt number for $R = 1$ and 5 is at most about 8 and 2% low, respectively, and 5% high for $R = 100$.

Temperature profiles in heat sources for local heating

As for the second heating condition; that is, local heating, the calculations are carried out for various heating positions. In these calculations, the values of R, L, and Gr^* are fixed to be 10, 15, and 8.2×10^4, respectively. Figure 8 shows the temperature profiles in the horizontal cross section at $X = 7.13$; i.e., the central position of heat source #9, while Figure 9 shows the peripheral distributions of surface temperature θ_w and heat flux F_w around the source of $\Delta Y/H_p = 1/4$, 2/4, and 3/4. Here, ΔY

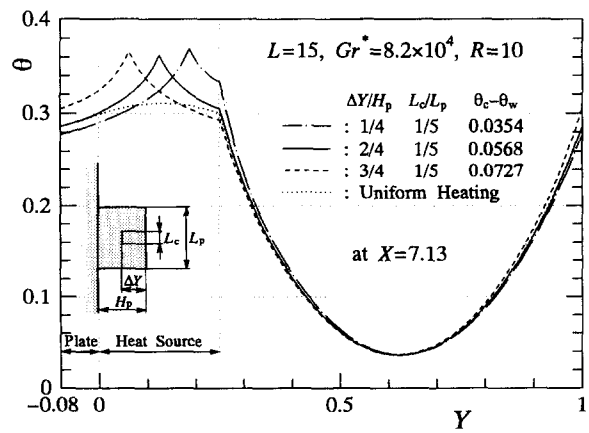

Figure 8 Effect of heating position on temperature profiles

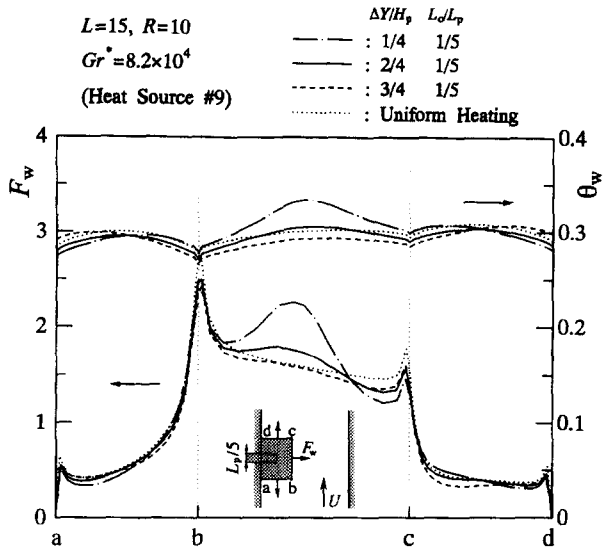

Figure 9 Peripheral distributions of heat flux and temperature

is the distance between the protrusion surface ($Y = 0.25$) and the concentrated heat source (see Figure 8).

The maximum temperature in the source θ_c is independent of the heating position, although the surface temperature θ_w is slightly varied with it. The surface temperature difference between the local and uniform heating conditions is about 11% at most for the case of the heating position nearest to the surface $\Delta Y/H_p = 1/4$. In addition, it is confirmed that the difference is reduced to 4% for $R = 20$. In this manner, the surface temperature under the local heating condition approaches that of the uniformly heated protrusion with increasing R. The same characteristics are also observed for the other heat sources. It is noted that the mean value of F_w is about 1, as estimated from Figure 9. This confirms that the present definition of q_w as the representative heat flux is valid. Furthermore, the heat generated from the source is almost evenly transferred to the front and back surfaces, as is also true in the case of uniform heating condition. Therefore, the Equation 11 obtained for uniform heating condition can also be applied to the case of local heating. As the thermal conductivity of real IC boards and packages is higher than the present numerical condition ($R = 10$), that is, $R = 12 \sim 85$ (MPE 1985), the surface temperature could be predicted better in a practical case by using Equation 11. Practically, when an approximate equivalent thermal resistance R_{cw} is given, the maximum temperature in the source θ_c can be predicted from Equation 11.

For the present case, the resistance R_{cw} is defined by heat transferred to the heat source surface Q_p as

$$R_{cw} = \frac{\Delta y}{\lambda_s A_p} = \frac{T_c - T_w}{Q_p} \tag{13}$$

To estimate R_{cw}, it is necessary to obtain an appropriate heat transfer area A_p with given Δy and λ_s. When the resistance R_{cw} is estimated by assuming $Q_p = Q_c/2$ (= half of heat generated in the chip), it is found that A_p should be $l_p/2$ to predict θ_c within an error of $\pm 10\%$.

Thermally optimum spacing of vertical parallel plates

In cooling technology for electronic equipment, it is of great importance to maintain the chip temperature of an IC package below a critical temperature. In this section, with reference to the thermally optimum analysis by Bar-Cohen and Rohsenow (1984), the optimum spacing of vertical parallel plates with discrete and protruding heat sources are discussed.

The total heat generation rate per plate Q is given by

$$Q = 2Aq_w = 2A\,\mathrm{Nu}_{l/2}\frac{\lambda_f}{h_e}\Delta T_{l/2} \tag{14}$$

where $\mathrm{Nu}_{l/2}$ and $\Delta T_{l/2}(= T_{w,l/2} - T_i)$ are the midheight Nusselt number and the midheight temperature difference, respectively. Using Equation 11 to determine $\mathrm{Nu}_{l/2}$ and dividing both sides of Equation 14 by the product of total area $2A$, plate spacing h, temperature difference $\Delta T_{l/2}$, thermal conductivity λ_f yields

$$\frac{Q}{2Ah\Delta T_{l/2}\lambda_f} = \frac{1}{h_p + h_e}\frac{2\xi^{1/2}h_e^{3/2}}{6.93} \times\left\{1 - \exp\left[-4.88(2\xi^{1/2}h_e^{5/2})^{-0.66}\right]\right\} \tag{15}$$

where

$$\xi = \frac{g\beta q_w}{\lambda_f \nu^2 l}\mathrm{Pr} = \frac{\mathrm{Gr}^*\mathrm{Pr}}{lh_e^4} \tag{16}$$

The product Ah in the term of left-hand side of Equation 15 is equal to the volume between adjacent plates. The term, therefore, represents the volumetric heat dissipation rate per unit temperature difference. On the other hand, the reciprocal of Equation 15; that is, $\Delta T_{l/2}/(Q/Ah)$, stands for the temperature rise per unit volumetric heat dissipation rate. Therefore, the thermally optimum spacing yielding the lowest $\Delta T_{l/2}$ for specified Q can also be estimated by Equation 15.

Figure 10 shows the relation between the heat dissipation rate $Q/(2Ah\Delta T_{l/2}\lambda_f)$ and the effective plate spacing h_e $(= h - h_p)$ for $Q = 7$W and $\xi = 6.5 \times 10^{11}$ m^{-5}. The lines show the calculated results by Equation 15, and the symbol represents those measured for central plate #3, where the effects of radiative heat transfer between the plates and to the ambient can be neglected (Fujii et al. 1992). In the present experiment, without the knowledge of the midheight temperature $T_{w,l/2}$, the arithmetic average of the eighth and the eleventh row package surface temperatures at $x = 0.14$ and 0.163 m (see Figure 3) is

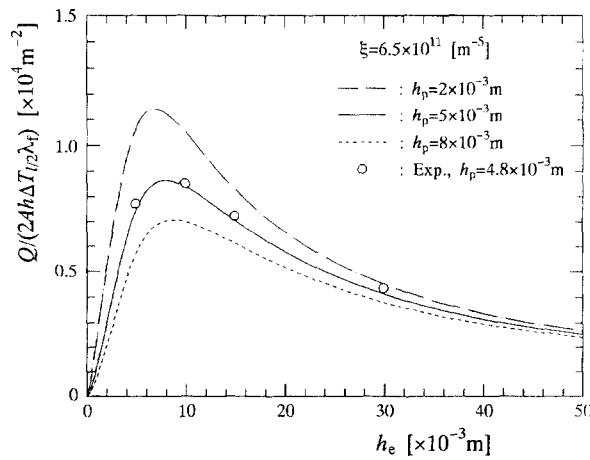

Figure 10 Relation between heat dissipation rate $Q/(2Ah\Delta T_{l/2}\lambda_f)$ and effective plate spacing h_e

used as $T_{w,l/2}$. The calculated result for $h_p = 5 \times 10^{-3}$ m agrees well with the measured ones for $h_p = 4.8 \times 10^{-3}$ m. From these calculated lines, the thermally optimum spacings h_{opt} ($= h_p + h_{e,opt}$) for $h_p = 2$, 5 and 8×10^{-3} m are estimated to be about 9, 13, and 17×10^{-3} m, respectively. In general, the h_{opt}s under arbitrary conditions are estimated using a differentiated relation $\{\partial[Q/(2Ah\Delta T_{l/2}\lambda_f)]/\partial h_e = 0\}$ of Equation 15.

Conclusions

Natural convection from an array of vertical parallel plates with discrete and protruding heat sources is studied theoretically and experimentally. The main conclusions are as follows.

(1) The present 2-D numerical results agree well with the experimental ones except for the large aspect ratio $L = 30$, where the 3-D effects become significant.
(2) The heat source surface temperatures can be predicted within an error of $\pm 20\%$ using Equation 11 with the effective spacing h_e as the characteristic length instead of the plate spacing h.
(3) There is no significant difference in the temperature and heat flux distributions at the heat source surface between the case of uniform and local heating in the sources. Consequently, the chip temperature of the practical IC packages can be estimated using Equations 11 and 13 when an equivalent thermal resistance is given. Within the present parameter ranges, the resistance is estimated with Equation 13 by taking $A_p = l_p/2$.
(4) The thermally optimum spacing h_{opt} yielding the lowest midheight temperature $\Delta T_{l/2}$ for specified heat generation rate Q can be estimated by Equation 15.

Acknowledgments

The authors acknowledge the valuable suggestions and discussions offered by T. Fujii of Toa University, and also thank W. Nakayama of Tokyo Institute of Technology and H. Yamamoto and the staff of Packaging Technology Dept. of Technology Development Div. of Fujitsu Ltd. for their provision of valuable data. K. Hamano assisted with the manufacture of the apparatus and took part in the experiments, and J. Qiao also took part in the numerical calculations.

References

Aihara, T. 1973. Effects of inlet boundary conditions on numerical solutions of free convection between vertical parallel plates. *Rpts. Inst. High Speed Mech.*, Tohoku Univ., **28**, 1–27

Aung, W. 1972. Fully developed laminar free convection between vertical plates heated asymmetrically. *Int. J. Heat Mass Transfer*, **15**, 1577–1580

Aung, W., Fletcher, L. S. and Sernas, V. 1972. Developing laminar free convection between vertical flat plates with asymmetric heating. *Int. J. Heat Mass Transfer*, **15**, 2293–2308

Bar-Cohen, A. and Rohsenow, W. M. 1984. Thermally optimum spacing of vertical, natural convection cooled, parallel plates. *J. Heat Transfer*, **106**, 116–123

Beckermann, C., Smith, T. F. and Pospichal, B. 1994. Use of a two-dimensional simulation model in the thermal analysis of a multi-board electronic module. *J. Electronic Packaging*, **116**, 126–133

Bodoia, J. R. and Osterle, J. F. 1962. The development of free convection between heated vertical plates. *J. Heat Transfer*, **84**, 40–44

Fujii, M. and Tomimura, T. 1988. Study on natural air cooling of IC board. *Proc. First KSME-JSME Thermal and Fluids Engineering Conference*, **2**, 330–335

Fujii, M., Tomimura, T., Gima, S. and Zhang, X. 1992. An experimental study of natural convection heat transfer from vertical parallel boards. In *Transport Phenomena Science and Technology*, B. X. Wang (ed.), Higher Education Press, Beijing, China, 153–158

Fujii, M., Tomimura, T., Zhang, X. and Gima, S. 1994a. An experimental study of natural convection from an array of vertical parallel plates. *Heat Transfer—Japan. Research*, **23**, 116–127

Fujii, M., Tomimura, T., Zhang, X. and Gima, S. 1994b. Natural convection from an array of vertical parallel plates. *Proc. 10th International Heat Transfer Conference*, **7**, 49–54

Incropera, F. P. 1988. Convection heat transfer in electronic equipment cooling. *J. Heat Transfer*, **110**, 1097–1111

Kim, S. H., Anand, N. K. and Fletcher, L. S. 1991. Free convection between series of vertical parallel plates with embedded line heat sources. *J. Heat Transfer*, **113**, 108–115

Miyatake, O. and Fujii, T. 1974. Natural convective heat transfer between vertical parallel plates with unequal heat fluxes. *Heat Transfer—Japan. Research*, **3**, 29–33

Modern Plastics Encyclopedia (MPE). 1985. **62**, 448–480

Nakayama, W. and Hirooka, Y. 1986. Natural convection cooled boards with different power loadings and IC package arrangements. *Proc. 23rd National Heat Transfer Symposium, Japan* (in Japanese), 406–408

Sparrow, E. M. and Gregg, J. L. 1956. Laminar free convection from a vertical plate with uniform surface heat flux. *Trans. ASME*, **78**, 435–440

Tomimura, T. and Fujii, M. 1988. Laminar mixed convection heat transfer between parallel plates with localized heat sources. In *Cooling Technology for Electronic Equipment*, W. Aung (ed.), Hemisphere Publishing Corporation, 233–247

Webb, B. W. and Hill, D. P. 1989. High Rayleigh number laminar natural convection in an asymmetrically heated vertical channel. *J. Heat Transfer*, **111**, 649–656